1142 *Chem. Mater.* **2010,** *22,* 1142–1148
DOI:10.1021/cm9021497

CHEMISTRY OF MATERIALS
Article

# Ionothermal Synthesis of Li-Based Fluorophosphates Electrodes†

N. Recham,‡ J-N. Chotard,‡ J-C. Jumas,§ L. Laffont, M. Armand,‡ and J-M. Tarascon*,‡

‡*LRCS - UMR 6007- Université de Picardie Jules Verne, 80039 Amiens, France, and* §*ICGM/AIME - UMR5253 - Université Montpellier II, 34095 Montpellier, France*

*Received August 7, 2009. Revised Manuscript Received September 29, 2009*

Fluoride-based materials have regained interest within the field of Li-ion batteries largely due to the advent of nanosizing which has transformed the insulating insertion compounds into attractive electrode materials. Herein we demonstrate the effectiveness of ionothermal synthesis in the preparation of nanometric $LiFePO_4F$ and $LiTiPO_4F$ phases with structures isotopic to tavorite $LiFePO_4(OH)$ at temperatures of only 260 °C, while temperatures of 600−700 °C are required to obtain coarse powders via the ceramic method. However, the redox-active phases, which are obtained in a high state of division, have lower redox voltages than $LiFePO_4$ despite the presence of fluorine. Additionally, $LiTiPO_4F$ shows staircase charge/discharge profiles with $Ti^{2/3+}$ and $Ti^{3/4+}$ couples. Though quite unusual in lithium intercalation oxides, a hint of a Li-driven $Fe^{3/4+}$ transition has been detected in $LiFePO_4F$.

## Introduction

Li-ion battery technology goes back to the early 1990s [1] with Sony's introduction of insertion compounds as electroactive materials for both positive and negative electrodes. Since then, advances made at both the electrode and electrolyte levels have been so tremendous that over the last 20 years their energy density has doubled to reach 200 W h/kg. Because of this high value and cycle life performance, Li-ion technology has conquered the portable electronic market and stands as a serious contender for electrical cars. However, for large-scale applications cost and safety issues must be overcome.[2] At the resources level, the cost is mainly determined by the element abundance; this is why materials based on sustainable 3d metal redox elements such as Mn ($LiMn_2O_4$, $LiMnPO_4$, $Li_2MnSiO_4$), Ti ($TiO_2$, $Li_4Ti_5O_{12}$, $Li_3Ti_7O_{12}$), and Fe ($LiFePO_4$, $Li_2FeSiO_4$) are receiving growing interest with respect to Co- or Ni-based electrodes.[3] Ironically, most of the phosphate and silicate based materials, which were disregarded 25 years ago because of their insulating properties, have turned out to be some of the best materials for electrodes (e.g., $LiFePO_4$).[4] This was made possible by the chemist's ability to develop new synthetic approaches, not only to make nanopowders of these insulating phases but also to carbon "nanopaint" these powders so as to provide a good electronic wiring.[5] This ability to turn insulating compounds into attractive electrode materials has rekindled interest in fluoride-based materials. Despite the fact that they are known to be poorer electronic conductors than their oxide counterparts, they display a greater potential owing to a larger ionicity of the M−F bond as compared to the M−O one.

Several fluoride based electrodes have resulted from this recent research, among which are $FeF_3$, $FeF_2$, and BiOF,[6] which react with Li via a conversion reaction mechanism, and $Na_2FePO_4F$,[7] $Li_5V(PO_4)_2F_2$,[8] and $LiVPO_4F$[9] in which the alkali metal can be reversibly extracted via a de/intercalation mechanism. The observation that the latter works at ≈ 4 V led Barker et al.[10] to synthesize most of the 3D-metal lithium fluorophosphate $LiMPO_4F$ phases (M = Fe, Ti, Co, Cr). The structures were then claimed, from undisclosed powder X-ray data, to be isostructural to Tavorite $LiFePO_4(OH)$,[11] but no electrochemical performances were mentioned.

These results give us the impetus to further explore the potential of $LiMPO_4F$ phases as potential electrode materials for Li-ion batteries. Fluoride based materials are generally made via solid-state reactions at high temperatures, and the $LiMPO_4F$ phases are no exception as they were made by reacting stoichiometric amounts of

† Accepted as part of the 2010 "Materials Chemistry of Energy Conversion Special Issue".

*Corresponding author. E-mail: jean-marie.tarascon@sc.u-picardie.fr.

(1) Nagaura; Tozawa, K. *Prog. Batteries Sol. Cells* **1990**, *9*, 209.
(2) Tarascon, J.-M.; Armand, M. *Nature* **2001**, *414*, 359–367.
(3) Armand, M.; Tarascon, J.-M. *Nature* **2008**, *451*(7179), 652–657.
(4) Padhi, A. K.; Nanjundaswamy, K. S.; Masquelier, C.; Okada, S.; Goodenough, J. B. *J. Electrochem. Soc.* **1997**, *144*(5), 1609–1613.
(5) Ravet, N.; Goodenough, J. B.; Besner, S.; Simoneau, M.; Hovington, P.; Armand, M. Presented at ECS Fall meeting, Hawaii, 1999, Abstract No. 127.
(6) (a) Amatucci, G. G.; Pereira, N. *J. Electrochem. Soc.* **2007**, *128*(4), 243–262.(4) , p.243-262. (b) Badway, F.; Mansour, A. N.; Pereira, N.; Al-Sharab, J. F.; Cosandey, F.; Plitz, I.; Amatucci, G. G. *Chem. Mater.* **2007**, *19*, 4129–4141.
(7) Ellis, B. L.; Makahnouk, W.R. M .; Makimura, Y.; Toghill, K.; Nazar, L. F. *Nat. Mater.* **2007**, *6*(10), 749–753.
(8) Barker, J.; Saidi, M. Y.; Swoyer, J. L. *J. Electrochem. Soc.* **2004**, *151*(10), A1670–A1677.
(9) Barker, J.; Saidi, M. Y.; Gover, R. K. B.; Burns, P.; Bryan, A. *J. Power Sources* **2007**, *174*(2), 927–931.
(10) Barker, J.; Saidi, M. Y.; Swoyer, J. L. International Patent WO0184655.
(11) Roberts, A. C.; Dunn, P. J.; Grice, J. D.; Newbury, D. E.; Dale, E.; Roberts, W. L. *Powder Diffraction* **1988**, *3*(2), 93–5.

 Published on Web 11/04/2009 

well selected precursors followed by several shake and bake steps[10]. The main drawback to ceramic synthesis, besides demanding a large amount of energy, is that it leads to highly polydisperse micrometer-sized powders, which results in poorly conducting materials. For this reason low temperature solvothermal/hydrothermal reactions conducted mainly in water are often preferred and have been used to great success in the preparation of electrochemically optimized $LiFePO_4$.[12,13] However, our ability to conduct solvothermal reactions in ionic liquids[14] rather than in water allows us to preserve the nanosize and monodispersed character of the obtained powders while offering an unprecedented opportunity to expand the way in which inorganic materials can be synthesized. We recently utilized[15] our ionothermal synthetic process in the successful low temperature elaboration of $Na_2MPO_4F$ (M = Fe, Mn). We describe herein how this process can be used to prepare, at mild temperatures, highly divided single-phased $LiMPO_4F$ (M = Ti, Fe) whose electrochemical performances will be described. In an effort to highlight the benefits of the ionothermal process over the ceramic process we have chosen to report each material's ceramic and ionothermal synthesis prior to presenting their electrochemical performances.

## Results and Discussion

**a. Ceramic Synthesis.** The $LiMPO_4F$ (M = Ti, Fe) were at first synthesized via a ceramic route which consists of first ball milling, for 10 min in a SPEX-type miller, stoichiometric amounts of the suitable $MF_3$ and $Li_3PO_4$ precursors to form 1 g of the desired $LiMPO_4F$. Precursors were chosen based on the ease of the foreseen reaction ($MF_3 + Li_3PO_4 \rightarrow LiMPO_4F + 2LiF$) owing to the strong lattice energy of LiF which acts as the driving force. The ball-milled powder was placed in either stainless steel (M = Ti) or platinum (M = Fe) containers, sealed under an argon atmosphere and heated at 700 °C for 24 h. The recovered powders were quickly rinsed with cold water to get rid of the formed LiF, washed with acetone, and oven-dried at 60 °C prior to being analyzed by X-ray diffraction. For both syntheses, the resulting powder turned out to almost be a single-phase with residual LiF despite the washes (Figure 1). All observed peaks could be indexed, except the peaks associated with LiF, in the previously reported space group $P\bar{1}$ (2) with the following lattice parameters $a$ = 5.1551(3) Å, $b$ = 5.3044(3) Å, $c$ = 7.2612(4)Å, $\alpha$ = 107.356(5)°, $\beta$ = 107.855(6)°, $\gamma$ = 98.618(5)°, and $V$ = 173.91(2) Å$^3$ for $LiFePO_4F$ (Figure 1a) and $a$ = 5.1991(2) Å, $b$ = 5.3139(2) Å, $c$ = 7.2428(3) Å, $\alpha$ = 106.975(3)°, $\beta$ = 108.262(4)°, $\gamma$ = 97.655(4)°, and $V$ = 176.10(2) Å$^3$ for $LiTiPO_4F$ (Figure 1c). It is worth mentioning that attempts to synthesize $LiFePO_4F$ in a stainless steel tube were not as successful owing to the partial reduction of $Fe^{3+}$ by Fe, hence, the need to use Pt tubing. In contrast, we did not encounter this problem with $LiTiPO_4F$ as $Ti^{(III)}$ is stable when in contact with $Fe^{0z}$.

**b. Ionothermal Synthesis.** To ensure the successful synthesis of single phased 3D-metal fluorophosphates, we designed our ionothermal synthesis around the chemical stability of the precursors and solvating properties of the ionic liquid with respect to those Li- and Fe-based precursors. Initially $MF_3$ and $Li_3PO_4$ were chosen as the precursors for this reaction because of the success of these compounds in the aforementioned ceramic approach. While basic affinity and redox considerations were useful in narrowing potential ionic liquids, ultimately a survey of various ionic liquids had to be conducted starting with the most classical one, 1-ethyl-3-methylimadozolium bis-(trifluoromethanesulfonyl imide) (EMI-TFSI). Reactions to identify the optimum conditions for $LiFePO_4F$ were conducted as follows: To 1 g of equimolar mixture of $FeF_3$ and $Li_3PO_4$ was added 5 mL of EMI-TFSI, the reaction was stirred for 20 min before being heated at 200 to 300 °C for 48 h, and finally the reaction was cooled down to room temperature. The recovered grey powders were (i) washed with 20 mL of acetone to get rid of traces in ionic liquid, (ii) rinsed in cold water to eliminate traces of LiF, which was expected to form during the synthesis, (iii) washed again with 20 mL of acetone, (iv) oven-dried at 60 °C, and (v) analyzed by X-ray. There was no evidence for the formation of $LiFePO_4F$ until 260 °C, which is also the temperature at which the $TFSI^-$ anion was found to undergo decomposition in the presence of $FeF_3$ with formation of elemental S (e.g., $H_2S$ smell) by an unknown mechanism, which caused the reduction of $Fe^{3+}$ in $Fe^{2+}$ and led to the formation of $LiFePO_4$ rather than $LiFePO_4F$. To eschew this issue, we decided to substitute the $TFSI^-$ anion for the very robust trifluoromethanesulfonate (triflate), which was found to be stable with respect to $FeF_3$. Using 1-butyl-3-methylimidazolium triflate and a synthetic temperature of 260 °C for 48 h, we succeeded in preparing single-phased $LiFePO_4F$ as deduced from XRD measurements (Figure 1b). Auspiciously the XRD Bragg peaks were broader than those found for the ceramic sample which is indicative of smaller particles; this was also confirmed by TEM measurements which show particle sizes as low as 20 nm (Figure 1f). This is in contrast with the ceramic process which produces particles ranging from 2 to 5 $\mu$m in size (Figure 1e).

A similar survey was conducted to determine the best ionic liquid for the synthesis of $LiTiPO_4F$ bearing in mind that (1) $Ti^{3+}$ is more stable than $Fe^{3+}$ so the $TFSI^-$ anion was not to be excluded and (2) that imidazolium starts to decompose in the presence of fluorides at temperatures near 280 °C probably due to the deprotonation of the acidic C2 proton. Therefore, we chose an ionic liquid protected at the C2 position with a methyl group and an OH (hydroxyl) group on the side chain to reduce the

(12) Chen, J.; Wang, S.; Whittingham, M. S. *J. Power Sources* **2007**, *174*, 442–448.
(13) Delacourt, C.; Poizot, P.; Levasseur, S.; Masquelier, C. *Electrochem. Solid-State Lett.* **2006**, *9*, A352–A355.
(14) Recham, N.; Dupont, L.; Courty, M.; Djellab, K.; Larcher, D.; Armand, M.; Tarascon, J.-M. *Chem. Mater.* **2009**, *21*(6), 1096–1107.
(15) Recham, N.; Chotard, J-N.; Dupont, L.; Djellab, K.; Armand, M.; Tarascon, J-M. *J. Electrochem. Soc.* **2009**, *156*, A993.

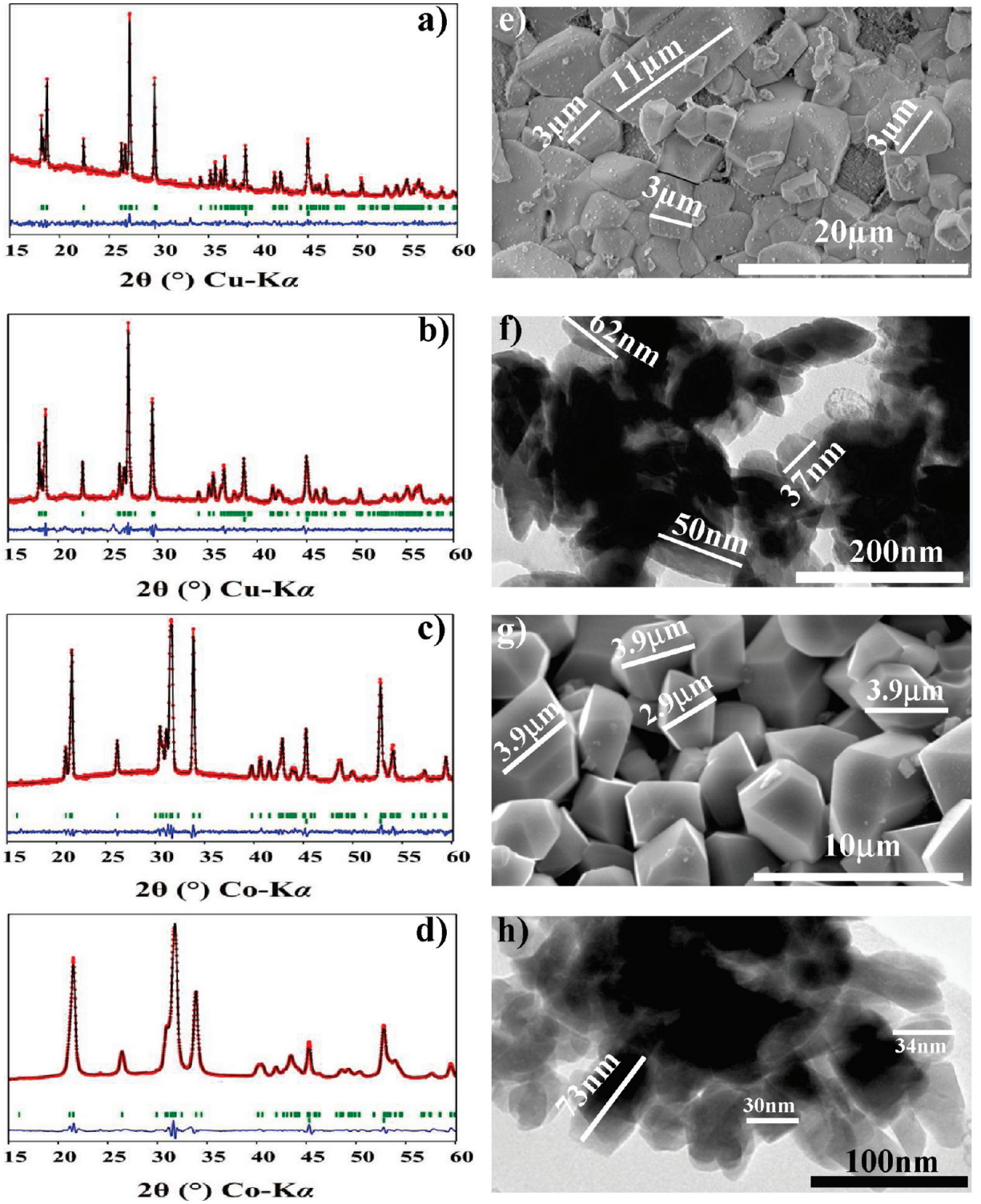


**Figure 1.** XRD powder patterns for the $LiFePO_4F$ and $LiTiPO_4F$ phases prepared by the ceramic (a, c) and ionothermal (b, d) processes, respectively, together with their corresponding morphology as deduced by SEM (e, g) and TEM (f, h).

reaction temperature via increasing the solubility of the precursors. The ionic liquid 1,2-dimethyl-3-(3-hydroxypropyl)imidazolium bis(trifluoromethane sulfonyl)imide was synthesized according to previous work. Using 5 mL of this ionic liquid in an autoclave, single-phased (Figure 1d) and nanosized $LiTiPO_4F$ powders (Figure 1h) were obtained after 48 h of heating at 260 °C while the ceramic process again produced micrometer size particles (Figure 1g).

At this point it is worth noting that, regardless of the type of ionic liquid used to carry out the synthesis, we have been able to obtain single-phased materials at temperatures as low as 260 °C as compared to the 700 °C necessary from a ceramic approach. This clearly demonstrates the great potential of ionothermal synthesis for inorganic materials once the proper ionic liquid has been identified. Further abounding about the positive attributes of ionothermal synthesis, we recall that early

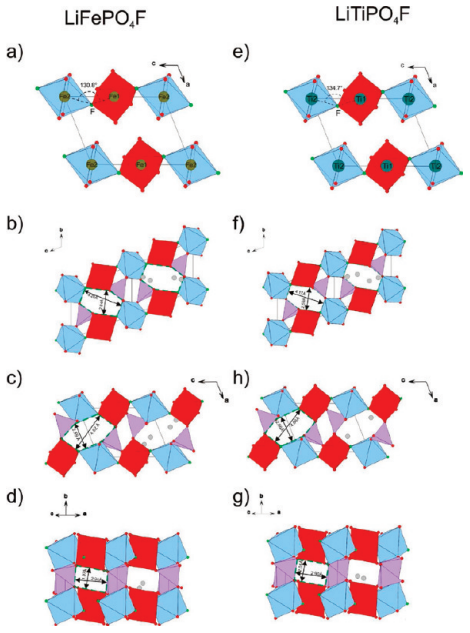


**Figure 2.** X-ray powder patterns of $LiFePO_4F$ (a) and $LiTiPO_4F$ (e). Experimental data (red dots), calculated pattern (black line), Bragg positions (green ticks), and difference curve (blue line) are shown. In both diagrams, first Bragg ticks correspond to the main phase $LiMPO_4F$ (M = Fe, Ti) while the second corresponds to LiF. Projections of $MO_4F_2$ octahedra chains (M = Fe, Ti) and resulting angles M1−F−M2. M1 and M2 centered octahedra are represented in red and blue in insets of Figures 3a,e, respectively. $LiMPO_4F$ structure projections along (b and f) the [100] direction, (c and h) the [010] direction, and (d and g) the [101] direction. Tunnels along those three directions are highlighted with green dashed lines as well as inner distances. $MO_4F_2$ octahedra are represented in blue and red while $PO_4$ tetrahedra are in purple. For clarity, lithium atoms in the tunnels at the left are omitted.

synthesis reports of tavorite ($LiFePO_4(F,OH)$ phases were calling for either a high temperature ceramic approach involving several (grinding + heating) steps or a hydrothermal approach, which necessitated 3 days of reaction at 400 °C and under 150 MPa.[16]

Although inherent to the use of ionic liquids and regardless of the type of materials we synthesized ($LiFePO_4F$ or $LiTiPO_4F$) or the nature of the ionic liquid we used, we could at the end of each experiment recover the ionic liquid so that it could be reused. Our recovery protocol consists first in washing the reaction supernatant with a concentrated HCl solution to get rid of ($LiFePO_4F$ or $LiTiPO_4F$) traces of powder which could remain after centrifugation. Afterward, the supernatant is washed with water to eliminate HCl traces and then diluted with dichloromethane ($CH_2Cl_2$) to separate it from water. Finally dichloromethane is stripped with a rotary evaporator, leaving behind the regenerated ionic liquid which can be used for subsequent experiments.

The structure of these phases has been reported [10] to be isostructural with $LiFePO_4(OH)$ [11], but no structural details have been given concerning the bond lengths or the Fe/Li environment. As such information is relevant to their electrochemical performances we decided to resolve their structure from powder data, as we could not grow single crystals. To perform such a study, the X-ray powder diffraction of each phase was recorded overnight on a Bruker D8 diffractometer using Cu Kα or Co Kα radiations (Cu $\lambda_1$ = 1.54053 Å; Cu $\lambda_2$ = 1.54431 Å, Co $\lambda_1$ = 1.78897 Å; Co $\lambda_2$ = 1.79285 Å) and equipped with a linear Vantec counter. The powder patterns were indexed (DICVOL04[17]) in a triclinic cell, (space group $P\bar{1}$). The structures were then refined using the Rietveld method with the Fullprof program,[18] starting with atomic coordinates found by FOX.[19] X-ray powder patterns, crystallographic data, and selected interatomic distances are shown in Figure 2a−e and Tables 1 and 2, respectively. This structure is built from transition metal centered octahedra $MO_4F_2$ (M = Fe, Ti) linked together by fluorine vertices in the trans position forming chains along the *c* axis. In both structures, two crystallographically independent metal sites are found in the unit cell

**Table 1. Lattice Parameters, Cell Volumes, and Atomic Coordinates for $LiFePO_4F$ and $LiTiPO_4F$[a]**

$LiFePO_4F$

| *a* (Å) | *b* (Å) | *c* (Å) | volume (Å$^3$) |
|---|---|---|---|
| 5.1551(3) | 5.3044(3) | 7.2612(4) | 173.91(2) |
| α | β | γ | |
| 107.357(5)° | 107.855(6)° | 98.618(5)° | |
| $\chi^2$ | $*R_p$ | $*R_{wp}$ | |
| 1.77 | 28.0 | 18.0 | |

| atom | Wyckoff position | *x* | *y* | *z* | occupation |
|---|---|---|---|---|---|
| Li1 | 2*i* | 0.38(5) | 0.68(5) | 0.83(4) | 0.5 |
| Li2 | 2*i* | 0.23(4) | 0.60(4) | 0.73(5) | 0.5 |
| Fe1 | 1*a* | 0(−) | 0(−) | 0(−) | 1 |
| Fe2 | 1*b* | 0(−) | 0(−) | 1/2(−) | 1 |
| P | 2*i* | 0.325(4) | 0.649(4) | 0.251(3) | 1 |
| O1 | 2*i* | 0.621(6) | 0.756(5) | 0.411(4) | 1 |
| O2 | 2*i* | 0.111(6) | 0.662(5) | 0.360(4) | 1 |
| O3 | 2*i* | 0.318(6) | 0.354(6) | 0.140(4) | 1 |
| O4 | 2*i* | 0.259(6) | 0.793(5) | 0.08(4) | 1 |
| F | 2*i* | 0.121(5) | 0.912(4) | 0.759(4) | 1 |

$LiTiPO_4F$

| *a* (Å) | *b* (Å) | *c* (Å) | volume (Å$^3$) |
|---|---|---|---|
| 5.1991(2) | 5.3139(2) | 7.2428(3) | 176.10(2) |
| α | β | γ | |
| 106.975(3)° | 108.262(4)° | 97.655(4)° | |
| $\chi^2$ | $R_p$ | $R_{wp}$ | |
| 2.23 | 15.7 | 12.0 | |

| atom | Wyckoff position | *x* | *y* | *z* | occupation |
|---|---|---|---|---|---|
| Li1 | 2*i* | 0.278(17) | 0.627(13) | 0.781(11) | 0.5 |
| Li2 | 2*i* | 0.232(14) | 0.584(15) | 0.609(11) | 0.5 |
| Ti1 | 1*a* | 0(−) | 0(−) | 0(−) | 1 |
| Ti2 | 1*b* | 0(−) | 0(−) | 1/2(−) | 1 |
| P | 2*i* | 0.3238(15) | 0.6372(13) | 0.2481(10) | 1 |
| O1 | 2*i* | 0.626(2) | 0.7579(19) | 0.3980(19) | 1 |
| O2 | 2*i* | 0.124(3) | 0.6670(19) | 0.373(2) | 1 |
| O3 | 2*i* | 0.330(2) | 0.351(2) | 0.1560(19) | 1 |
| O4 | 2*i* | 0.259(2) | 0.784(2) | 0.0996(17) | 1 |
| F | 2*i* | 0.1074(19) | 0.9171(16) | 0.7627(14) | 1 |

[a] The given reliability factors, $*R_p$ and $*R_{wp}$, are relatively high for the Fe-based compound owing to the large background in our collected data that we have not corrected for.

(16) Genkina, E. A.; Kabalov, Y. K.; Maksimov, B. A.; Mel′nikov, O. K. *Kristallografiya* **1984**, *29*, 50.

(17) Boultif, A.; Louër, D. *J. Appl. Crystallogr.* **2004**, *37*, 724.
(18) Rodriguez-Carvajal, J. *Physica B* **1993**, *192*, 55.
(19) Favre-Nicolin, V.; Cerny, R. *J. Appl. Crystallogr.* **2002**, *35*, 734 (see also: http://objcryst.sourceforge.net).

**Table 2. Selected Interatomic Distances (Å) and Angles (deg) in $LiFePO_4F$ and $LiTiPO_4F$**

| | $LiFePO_4F$ | | | $LiTiPO_4F$ | |
|---|---|---|---|---|---|
| Fe1 | O1(×2) | 1.97(3) | Ti1 | O1(×2) | 1.965(9) |
| | O2(×2) | 2.04(3) | | O2(×2) | 2.029(13) |
| | F(×2) | 2.01(3) | | F(×2) | 2.004(10) |
| | F−Fe1−O1 | 90.6° | | F−Ti1−O1 | 90.5° |
| | F−Fe1−O2 | 90.6° | | F−Ti1−O2 | 92.8° |
| | O1−Fe1−O2 | 93.0° | | O1−Ti1−O2 | 93.0° |
| Fe2 | O3(×2) | 2.04(3) | Ti2 | O3(×2) | 2.098(9) |
| | O4(×2) | 1.93(3) | | O4(×2) | 1.984(11) |
| | F(×2) | 1.98(3) | | F(×2) | 1.92(11) |
| | F−Fe2−O3 | 91.6° | | F−Ti2−O3 | 90.5° |
| | F−Fe2−O4 | 98.2° | | F−Ti2−O4 | 94.0° |
| | O3−Fe2−O4 | 91.3° | | O3−Ti2−O4 | 90.5° |
| P | O1 | 1.50(4) | P | O1 | 1.521(11) |
| | O2 | 1.54(4) | | O2 | 1.574(19) |
| | O3 | 1.52(4) | | O3 | 1.481(12) |
| | O4 | 1.58(4) | | O4 | 1.487(15) |
| Li1 | O1 | 2.4(3) | Li1 | O1 | 2.29(7) |
| | O2 | 2.6(2) | | O2 | 2.17(6) |
| | O3 | 1.6(3) | | O3 | 1.92(7) |
| | O4 | 2.1(3) | | O4 | 2.25(8) |
| | F | 2.0(3) | | F | 1.89(8) |
| Li2 | O1 | 2.2(2) | Li2 | O1 | 2.04(8) |
| | O2 | 1.9(2) | | O2 | 1.82(9) |
| | O2 | 2.7(4) | | O2 | 2.19(8) |
| | O3 | 2.2(2) | | O3 | 2.28(7) |
| | O4 | 2.4(3) | | F | 2.10(8) |
| | F | 1.8(2) | | | |

**Table 3. $^{57}$Fe Mössbauer Hyperfine Parameters of $LiFePO_4F$, $Li_{1+x}FePO_4F$, and $Li_{1-x}FePO_4F$[a]**

| sample | δ (mm/s) | Δ (mm/s) | Γ (mm/s) | contribution (%) | attribution |
|---|---|---|---|---|---|
| $LiFePO_4F$ | 0.433(5) | 1.058(9) | 0.272(4) | 50 | Fe(III)1 |
| | 0.430(5) | 1.174(9) | 0.272(4) | 50 | Fe(III)2 |
| $Li_{1+x}FePO_4F$ | 0.42(1) | 1.07(3) | 0.43(5) | 31 | Fe(III) |
| $x \approx 0.2$ | 1.25(1) | 2.71(1) | 0.43(5) | 49 | Fe(II) |
| | 1.25(1) | 2.07(1) | 0.43(5) | 20 | Fe(II) |
| $Li_{1-x}FePO_4F$ | 0.43(1) | 1.13(1) | 0.29(5) | 93 | Fe(III) |
| $x \approx 0.1$ | 0.13(3) | 0.17(4) | 0.29(5) | 7 | Fe(IV) |

[a] δ = isomer shift vs α-Fe, Δ = quadrupole splitting, Γ = line width.

(labelled Fe1 and Fe2 for $LiFePO_4F$ (Figure 2a, inset) and Ti1 and Ti2 for $LiTiPO_4F$ (Figure 2e, inset). Consequently, the $MO_4F_2$ chains along the *c* axis constitute an alternation of M1 and M2 centered octahedra. These octahedra are slightly distorted with angles in the range 90.6−98.2° (Table 2). The $^{57}$Fe Mössbauer spectrum for $LiFePO_4F$, as shown by an isomer shift of 0.43 mm/s vs α-Fe, is characteristic of $Fe^{3+}$ with therefore a barely asymmetric quadrupole doublet, which confirms slightly different Fe sites. The robustness of the fitting was improved by introducing two Fe sites with slight different QS and IS (Figure 4a, Table 3) which is in good agreement with the structural findings. Regarding the nature and thus the size of the metal, those chains are more or less tilted, the Fe1−F−Fe2 angle being 130.8° compared to the Ti1−F−Ti2 angle of 134.7° (Figure 2a,e insets). Each oxygen from the equatorial plane of the octahedron is common to a $PO_4$ tetrahedron bridging the $MO_4F_2$ chains, leading to the formation of a three-dimensional framework and delimiting three tunnels along the [100], [010], and [101] directions where the $Li^+$ ions lie on the edges (Figure 2b−g). Regardless of the metal (Ti or Fe), the tunnels along the [100] (Fe: 4.20 Å × 2.64 Å; Ti 4.17 Å × 2.59 Å) and [010] (Fe: 4.02 Å × 2.59 Å; Ti 4.06 Å × 2.66 Å) directions are larger than the third one along the [101] (Fe: 1.97 Å × 2.94 Å; Ti 2.05 Å × 2.90 Å) and constitute probably the main diffusion path for lithium. Along that line, the appreciable ionic conductivity reported for the $LiMgSO_4F$ ($\sigma = 5 \times 10^{-8}$ S·cm$^{-1}$ at 200 °C and $E_a$ = 0.94 eV), which adopts the same tavorite-type structure, does not come as a total surprise.[20]

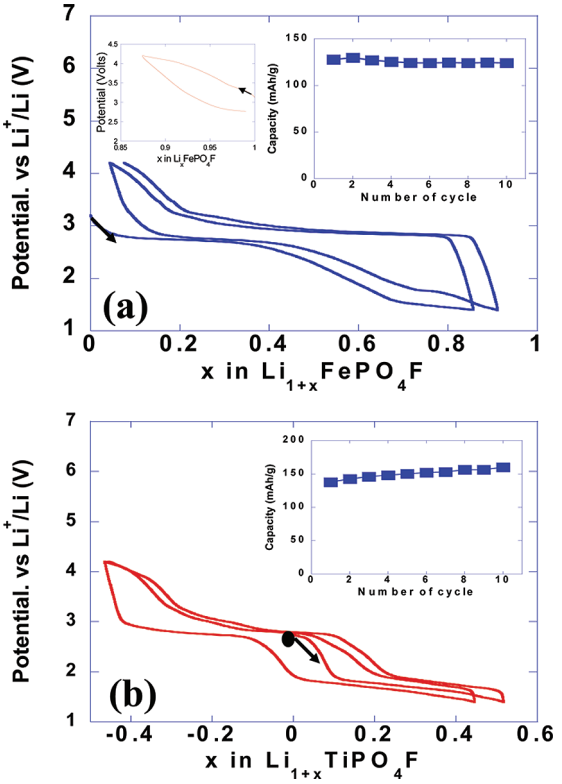


**Figure 3.** Voltage−composition curve for (a) Li/$LiFePO_4F$ and (b) Li/$LiTiPO_4F$ cells using ionothermally made positive electrodes, together with their corresponding cycling capacity retention as inset. The cells were cycled at a C/15 rate. The voltage−composition curve for a $LiFePO_4F$, which has been started toward oxidation, under the same C/15 current conditions, is shown as an inset in (a).

**c. Electrochemistry.** Turning to the electrochemical performances, the samples were investigated in Li-half Swagelok cells assembled in an argon drybox. Prior to being used as positive electrodes, the active materials were ball milled with a 15% weight ratio of SP carbon. The cells were loaded with 6−8 mg/cm$^2$ of active material as the positive electrode and 1 cm$^2$ Li disks as the negative electrode and were cycled in $LiPF_6$-based EC-DMC electrolyte between 1.5 and 4.5 V (Figure 3b). For reasons of concision the data will only be reported for the ionic liquid samples; this data shows similar voltage−composition profiles to those of their ceramic counterparts but far better kinetics (e.g., less polarization between charge and discharge), owing to their highly divided states. The voltage composition curve of $LiTiPO_4F$ shows a staircase

(20) Sebastian, L.; Gopalakrishnan, J.; Piffard, Y. *J. Mater. Chem.* **2002**, *12*, 374–377.

variation with two pseudo-plateaus located near 2.9 and 1.7 V. These plateaus correspond to the oxidation of $Ti^{3+}$ into $Ti^{4+}$ and the reduction of $Ti^{3+}$ into $Ti^{2+}$ when departing from $x = 1$ in charge or discharge, respectively. This process is fully reversible, and Li/$LiTiPO_4F$ can cycle over a $\Delta x$ of 1 leading to a sustained reversible capacity of 150 mA h/g (Figure 3b, inset). At this point it should be recalled that a similar staircase voltage curve centered near $x = 1$ with two plateaus at 4.2 V ($V^{+3} \leftrightarrow V^{4+}$) and 1.8 V ($V^{+3} \leftrightarrow V^{+2}$) was reported for the isostructural $LiVPO_4F$ phase [8]. However, essential differences are noted (1) on the amplitude of these plateaus, which are limited to about $x = 0.5$ on either side in our case while they were shown to extend up to $x = 0.8$ for the V-based phase, and (2) on the larger voltage hysteresis for the pseudo plateaus cross-over.

The $LiFePO_4F$ phase was found to be electrochemically active as well (Figure 3a) with a redox voltage centered around 3 V and a sustained reversible capacity of about 0.85 Li (e.g., 150 mA h/g) per unit formula. Nevertheless, the curve is atypical with the presence of a staircase discharge for $LiTiPO_4F$ that seems to be absent from the subsequent charge while it resurfaces in the second discharge. This is related to structural transitions with the appearance of a low temperature phase having limited kinetics with respect to the first one, so that upon oxidation its potential approaches that of the first one, hence hindering its straight appearance in the charging voltage profile. Our discharge cut off voltage may sound arbitrary, but it is not, because it is the result of studying the reversibility of several Li/$LiFePO_4F$ cells as a function of their discharge voltages. It was found that extending the discharge below 1.4 V triggered a conversion-type reaction leading to the presence of Fe metal as determined by Mössbauer measurements (not shown here).

Additionally, we explored the feasibility of electrochemically oxidizing $LiFePO_4F$, which implies the rarely encountered oxidation of $Fe^{3+}$ to $Fe^{4+}$. Surprisingly, we observed (Figure 3a inset), although limited, some reversible capacity ($\Delta x \approx 0.1$) suggesting the feasibility of such an option. To tests this hypothesis Mössbauer spectra were recorded for the oxidized ($x \approx -0.1$) and partially reduced ($x \approx 0.80$) sample. For the oxidized sample $Li_{0.9}FePO_4F$, the Mössbauer spectrum shows a slight asymmetric doublet (Figure 4c). Successful fitting of the spectrum has been realized with two sub-spectra: the first one which dominates, with hyperfine parameters $\delta = 0.43$ mm/s and $\Delta = 1.13$ mm/s, is characteristic of pristine $LiFePO_4F$ while the second one, with a weak contribution (7%) to the total absorption and hyperfine parameters $\delta = 0.13$ mm/s and $\Delta = 0.17$ mm/s, reveals a change in the oxidation state of iron. Such values of isomeric shifts (IS) in the range of $-0.15$ to 0.15 mm/s

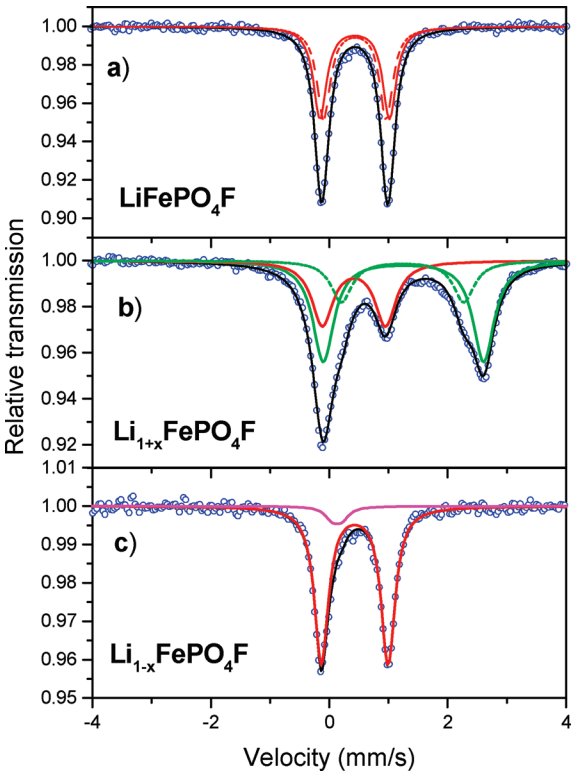


**Figure 4.** $^{57}$Fe Mössbauer spectra of $LiFePO_4F$ (a), $Li_{1+x}FePO_4F$ ($x \approx 0.8$) (b) and $Li_{1-x}FePO_4F$ ($x \approx 0.1$) (c).

are typical of the $Fe^{4+}$ state,[21−23] so we can attribute these second subspectra to oxidized $Fe^{4+}$. The reduced ($x \approx 0.80$) sample shows the typical spectra for $Fe^{3+}$ as a pristine material, which accounts for 30% of the total absorption, together with two quadrupole doublets having similar isomer shift parameters ($\delta = 1.25$ mm/s, $\Delta = 2.71$ mm/s; $\delta = 1.24$ mm/s, $\Delta = 2.07$ mm/s) but a different contribution (49 and 20%, respectively), indicative of two non-equivalent $Fe^{2+}$ sites (Figure 4b, Table 3). The structural changes associated with Li insertion/deinsertion into both $LiTiPO_4F$ and $LiFePO_4F$ phases have been studied by in situ XRD measurements. The details of this study, together with an in situ Mössbauer study of the Fe-based phase, have revealed the appearance of structural phase changes for each staircase voltage change.

Obviously, these phases do not compare positively with respect to $LiFePO_4$, which has become the benchmark material for the battery community for two reasons: (1) they display staircase voltage composition dependence as opposed to the single insertion voltage displayed by $LiFePO_4$ and are preferred for applications though charge monitoring is more complex, and (2) they show a lower redox voltage leading to lower energy density. This last point is somewhat worth a thought as it reminds us that F-based compounds do not systematically imply an increase in potential. It does for isotypic compounds only, as witnessed by the increase in the redox voltage when

(21) Menil, F. *J. Phys. Chem. Solids* **1985**, *46*, 763–789.
(22) Waerenborgh, J. C.; Rojas, D. P.; Vyshatko, N. P.; Shaula, A. L.; Kharton, V. V.; Marozau, I. P.; Naumovich, E. N. *Mater. Lett.* **2003**, *57*(28), 4388–4393.
(23) Presniakov, I.; demazeau, G; Boranov, A.; Sobolev, A.; Pokholok, K. *Phys. Rev. B* **2005**, *71*, 054409.
(24) Groguenec, L.; Marx, N.; Carlier, D.; Wattiaux, A.; Bourgeois, L.; Kubiak, P.; LeCras, F.; Delmas, C. Presented at the ACS Meeting, Cleveland, OH, May 20−23, 2009; CRM-100.

moving from the $LiFePO_4(OH)$ phase (2.6 V) [24] to $LiFePO_4F$ (3.0 V).

## Conclusions

In summary this work has further confirmed the benefits of ionothermal over ceramic synthesis in preparing highly divided $LiFePO_4F$ and $LiTiPO_4F$ materials, although the synthesized materials fall short of meeting $LiFePO_4$ performances. Therefore, their rich crystal chemistry provides a valuable asset in the hunt for better positive electrode materials.

**Acknowledgment.** We would like to thank M. Courty for having performed TGA/DSC measurements not reported in the paper, K. Djellab for his assistance in taking SEM/TEM pictures, Elena M. Arroyo for sharing preliminary calculations on these materials, and members of the ALISTORE-ERI nanopositive team for fruitful discussions.